Pergamon

Cement and Concrete Research 33 (2003) 155–164

CEMENT AND CONCRETE RESEARCH

Porosity, pore size distribution and in situ strength of concrete

Rakesh Kumar[a], B. Bhattacharjee[b,*]

[a]Bridges Division, Central Road Research Institute, New Delhi 110 020, India
[b]Department of Civil Engineering, Indian Institute of Technology-Delhi, Hauz Khas, New Delhi 110 016, India

Received 23 July 1997; accepted 24 July 2002

Abstract

In this study, in situ strength of concrete was determined through compression test of cores drilled out from laboratory cast beams. The apparent porosity and pore size distribution of the same concrete were determined through mercury intrusion porosimetry, performed on small-drilled cores. The normal-strength concrete mixes used in the experimental investigation were designed to exhibit a wide variation in their strengths. To ensure further variation in porosity, pore size distribution and strength, two modes of compaction, two varieties of coarse aggregates, different levels of age, curing period and exposure condition of concrete were also introduced in experimental scheme. With the data so generated, an appraisal of the most frequently referred relationships involving strength, porosity and pore size of cement-based materials was carried out. Finally, a new empirical model relating the in situ strength of concrete with porosity, pore size characteristics, cement content, aggregate type, exposure conditions, etc., is presented.

Keywords: Mercury porosimetry; Pore size distribution; Pore system; Concrete; Cement content

1. Introduction

Concrete prepared with hydraulic cement binder can be regarded as a chemically bonded ceramic. The hydration reaction of cement results in a product consisting of solid and a pore system [1]. Pores are thus inherent to concrete. Pores in concrete can also result from inadequate compaction. This pore system governs the most important properties of concrete, notably its strength [2,3]. Well-compacted concrete prepared with hard low-porosity aggregates may be assumed to be a multiphase material consisting of coarse aggregates embedded in mortar matrix. The mortar matrix consists of fine aggregates, the solid cement hydrates, unhydrated cement, etc., and the pore system [4]. The pore system present in the mortar of concrete, however, is markedly different from the pores of well-compacted mortar prepared independently using identical proportions of the relevant ingredients. The above difference in the two pore systems is due to the transition zone pores present at mortar–aggregate interface [5–7]. Capillary porosity of hardened cement paste depends on water-to-cement ratio. Water–cement ratio also governs the transition zone porosity in concrete [4]. Thus, there are a number of well-established strength versus water–cement ratio relationships, which indirectly relate the strength of concrete with its pore system characteristics [4,8,9]. These relationships serve their purpose very well in the design of concrete mixes. A few of these relationships take into account air content and degree of hydration of concrete. However, such indirect relationships do not take into account the pores present in hardened concrete in structure due to inadequate compaction, etc. Further, the pore system in concrete also changes with degree of hydration and chemical changes due to aggressive environments, etc. A direct relationship, on the other hand, can facilitate the strength estimation of in situ concrete from the knowledge of its pore system characteristics. For the purpose of mix design, however, strength/water–cement ratio relationships are more useful. The most important characteristics of pore system are porosity and pore size distribution, which can be determined through mercury intrusion porosimetry (MIP). However, MIP results are affected by a number of factors and the same must be suitably accounted for in the experimental procedure adopted [10–14]. Secondly, the smallest size of pore, in which mercury can intrude, depends upon the maximum intrusion pressure applied. Consequently, extent of porosity that can

* Corresponding author. Tel.: +91-11-6591193; fax: +91-11-6862037.
E-mail address: bishwa@civil.iitd.ernet.in (B. Bhattacharjee).

0008-8846/03/$ – see front matter © 2003 Elsevier Science Ltd. All rights reserved.
PII: S0008-8846(02)00942-0

be determined by porosimetry test depends upon the nature of the pores, the size of the smallest pore likely to be encountered in the material and the maximum intrusion pressure applied.

The pore system in cement-based materials consists of four types of pores. These are: (a) gel pores, which are micropores of characteristic dimension 0.5–10 nm; (b) capillary pores, which are mesopores with average radius ranging from 5 to 5000 nm; (c) macropores due to deliberately entrained air; and (d) macropores due to inadequate compaction. In concrete, in addition to the above pores, there can be cracks at aggregate–mortar interface due to shrinkage. The gel pores, which are mostly of 1.5–2.0 nm size, do not influence the strength of concrete adversely through its porosity, although these pores are directly related to creep and shrinkage. Capillary pores and other larger pores, on the other hand, are responsible for reduction in strength and elasticity, etc. [4,7,15–17]. Thus, while dealing with an empirical strength–porosity relationship of concrete, contribution of the gel pores in the overall porosity and pore size distribution of concrete can be neglected, without introducing any significant error. Hence, to determine the pore system characteristics influencing the strength, the maximum pressure in the porosimetry test must be sufficient to cause intrusion of mercury in the smallest capillary pore. In mercury porosimetry, a major part of gel pores remains nonintruded. Further, the closed pores also remain nonintruded. One other limitation pointed out as regard to mercury porosimetry is that it measures entry sizes rather than true pore size that is related to ink bottle effect [18]. Thus, the porosity determined, as above, is apparent porosity.

A number of relationships relating strength of cement-based materials with their pore system characteristics are available in the literature. In this paper, firstly, the results of an experimental investigation are presented, whereby data on in situ cube compressive strength of concrete—estimated through compression test of cores drilled out from laboratory cast beams—are generated, together with MIP data for the same concrete. This is followed by an appraisal whereby most frequently referred relationships involving strength and pore system characteristics of cement-based materials are evaluated for their suitability in strength estimation of in situ concrete. Finally, a new empirical relationship for in situ strength of concrete is proposed, which takes apparent porosity, pore size characteristics (corresponding to 33,000 psi intrusion pressure) and binder content of the concrete into account.

2. Experimental investigation

2.1. Objectives and scope

The main objectives of this experimental investigation were to generate sufficient data on strength, apparent porosity and pore size distribution of concrete. It was also desired that the strength data so generated should adequately cover the range of strength usually encountered for normal-strength concrete. High-strength concrete, produced using water-reducing agent and pozzolanic microfiller, was left out of the scope of this work.

2.2. Mix proportions and experimental factors

Strength and porosity of concrete depend upon water–cement ratio. Considering the practical limits of water–cement ratios (0.38–0.65) for workable concrete prepared without water-reducing agent, six concrete mixes were designed so as to ensure adequate variation in strength. Same ordinary Portland cement was used throughout this investigation. Similarly, throughout the investigation, the same land-quarried local sand confirming the Zone II of British Standard and potable laboratory tap water were used as fine aggregate and mixing water, respectively. To ensure further variation in strength and porosity, two modes of compaction, namely, compaction through mechanical vibration and manual compaction through tamping rod, were adopted in the experimental programme. Two types of graded coarse aggregates of 20 mm maximum size were also used: one being the crushed quartzite rock while the other was obtained in the laboratory by crushing common surface clay bricks. The former was hard with negligibly small porosity and the latter was soft and porous with a water absorption value of 13.7%.

Degree of hydration, i.e., the age, curing, exposure to aggressive environment, etc., also affects the strength and pore system of concrete. Thus, further variation in strength, porosity and pore size distribution of concrete was ensured by adopting the age, curing period, exposure to acidic water and thermal exposure as experimental factors. Two levels of age, namely, 28 and 84 days, and two levels of curing period, i.e., moist curing for 1 and 27 days, were also used. Similarly, two levels of exposure conditions, namely, exposure to open air and exposure to acidic environment of pH 4–5, and three levels of thermal exposure, i.e., exposure to 26 (room temperature), 300 and 600 °C were used. As factorial experiment design would have resulted in a large number of samples, the levels of the factors were adopted in a restricted way. Details of the samples prepared are given subsequently.

2.3. Casting

Thirty-two concrete beams of dimensions $1000 \times 200 \times 100$ mm as shown in Fig. 1 were cast using six designed mixes designated as Mix1–Mix6. Four more beams were also cast using crushed brick coarse aggregates instead of quartzite aggregates. The mix proportions used for casting these beams were the same as those of Mix1 and Mix2, except that additional absorption of water by the aggregates was also accounted for in this case. These mixes are designated as Mix7 and Mix8, respectively. Half of the total

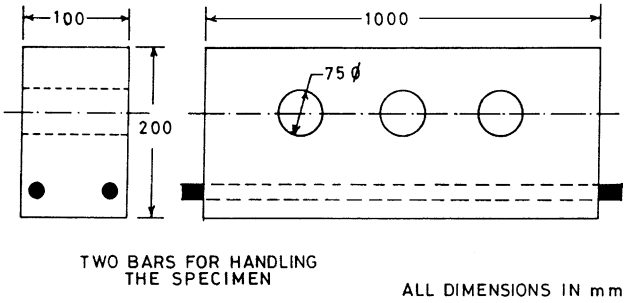

Fig. 1. Concrete beam specimen.

number of beams cast with each mix was compacted through mechanical mode of compaction (using immersion-type needle vibrator) and the other half was compacted manually with the help of a 25-mm-diameter tamping rod. These modes of compaction are abbreviated as VC and HC, respectively. All the beams were demoulded after 24 h of casting and cured as explained in Section 2.4.

2.4. Curing and exposure conditions

To ensure adequate curing, the beam specimens after demoulding were wrapped under wet hessian cloth, wetted continuously by sprinkling water. Most of the beams were cured for 27 days, but a few beams were cured for 1 day and left exposed to atmosphere prior to sample extraction. Some of the beams after 27 days of curing were submerged in acidic water (pH 4–5) for a period of 84 days. Due to size restriction of the furnace, cores drilled out from some of the beams, instead of beams themselves, were subjected to 300 and 600 °C temperatures. The details of concrete mix proportions, cube compressive strength of concrete, number of beams, etc., are presented in Table 1.

2.5. Test for in situ compressive strength

In situ strength of concrete in beams was determined through core test. From each beam, three cores, 75 mm in diameter and 100 mm in length, were drilled. The cores were drilled perpendicular to the direction of the casting as shown in Fig. 1. The compression test on dry cores was conducted on universal testing machine by ensuring a rate of loading of 12 MPa/min as per standard practice [19,20]. The representative in situ cube strength of concrete in the beams was estimated from average failure load of three cores according to Eq. (1) [20]:

$$f_{cu} = \frac{2.5 f_{\lambda}}{1.5 + 1/\lambda}. \quad (1)$$

In Eq. (1), f_{cu} is the estimated in situ cube compressive strength; f_{λ} is the determined cylinder compressive strength of a core with length/diameter = λ. For the present study, λ was 4/3 for all the cores.

2.6. MIP

A number of factors affect the MIP results. Most important among them are the method of sampling, number of sample, sample conditioning, rate of pressure application, maximum intrusion pressure applied, values of contact angle and surface tension of mercury used in Washburn's equation, etc. [11]. Again, the dimensions of the penetrometer restrict the maximum size of the sample used in MIP. Hence, only small samples in the form of core, crushed chunk, tablets, etc., can be used in porosimetry. Therefore, to obtain representative results, within desirable accuracy, the sample size, i.e., number of samples to be used for a given concrete specimen, needs to be statistically ascertained. Therefore, prior to actual investigation, a preliminary experimental investigation was carried out before arriving at a suitable method of sample collection, number of sample to be tested, form of the sample, rate of pressure application, etc. [10–12]. Further, for this study, contact angle and surface tension values of mercury were adopted from available literature. In addition to the above major factors, certain minor factors—such as expansion of sample cell under pressure, differential mercury compression, sample compression and hydrostatic head of mercury, etc.—also affect the MIP results to a limited extent. The effects of these factors are of minor consequences; hence, their affects were neglected [11].

2.6.1. Sample preparation, number of sample and conditioning and tests parameters

The number of samples required in MIP to obtain the average value of porosity and mean distribution radius (defined later) within ±15% accuracy was obtained sta-

Table 1
Mix proportions and details of concrete beam specimens cast

Mix proportions (C:S:A:w/c)	Mix designation	Coarse aggregate type	28-Day cube compressive strength (MPa)	Number of beam cast using modes of compaction	
				VC	HC
1:2.5:5.1:0.65	Mix1	Quartzite	31	1	1
1:2.2:4.2:0.56	Mix2	Quartzite	34	7[a]	7[a]
1:1.8:3.9:0.51	Mix3	Quartzite	35	1	1
1:1.5:3.6:0.46	Mix4	Quartzite	38	1	1
1:1.3:3.2:0.42	Mix5	Quartzite	43	1	1
1:1.1:2.7:0.38	Mix6	Quartzite	45	5[b]	5[b]
1:2.5:5.1:0.65	Mix7	Broken brick	14	1	1
1:2.2:4.2:0.56	Mix8	Broken brick	16	1	1

[a] Includes: 1(27 days cured and tested on 28th day) + 1(1 day cured and tested on 28th day) + 1(27 days cured and tested on 84th day) + 1(1 day cured and tested on 84th day) + 1 (27 days cured and subjected to acidic environment) + 1(27 days cured and subjected to 300 °C) + 1(27 days cured and subjected to 600 °C) = 7.

[b] Includes: 1(27 days cured and tested on 28th day) + 1(27 days cured and subjected to acidic environment) + 1(27 days cured and subjected to 300 °C) + 1(27 days cured and subjected to 600 °C) + 1(1 day cured and tested on 84th day) = 5.

tistically using Stein's two-stage formula. This was found to be six [10–12]. Thus, six numbers of samples were tested and average results were taken as the representative of a concrete specimen. Preliminary investigation carried out revealed that a small-cored sample of the concrete is the most appropriate form for MIP study [10–12]. It was also observed that rate of pressure application has little effect on the measured porosity and pore size distribution [10–12]. This was also confirmed by other research works [21,22]. Therefore, in this study, six small cores of 25 mm diameter and 15–25 mm length were drilled out from each of the concrete beams. Oven drying is reported to be the best method for sample conditioning and the corresponding contact angle to be adopted is 117° [10,13,14]. Therefore, the samples were dried in an oven at 105–110 °C for 24 h and stored in a desiccator prior to testing.

2.6.2. Testing

Testing was performed on Quantachrome Autoscan-33 mercury porosimeter having a pressure range from subambient to 33,000 psi. The contact angle and the surface tension of mercury were assumed to be 117° and 0.484 N/m, respectively, for the oven-dried samples [10]. Consequently assuming the cylindrical pores, the Washburn's equation yields:

$$r = 63,750/p \tag{2}$$

where p is in pounds per square inch and r is in nanometer. With this pressure, the smallest size of pore into which mercury can be intruded is 2 nm. Thus, the pressure is sufficient to ensure intrusion of mercury in all the capillary pores, as the reported radius of the smallest size capillary pore is 5 nm. However, majority of the gel pores would remain nonintruded. The largest radius (pore size) that can be accounted for in the pore size distribution is 0.2 mm with subambient pressure filling apparatus. The sample cell fitted with the base cell of capacity 17.7 cm^3 was used throughout the experiment. Six numbers of samples were tested for given concrete to ensure adequate accuracy of the MIP results representing particular concrete. All tests were performed at a constant moderate scanning rate indicated by Point 5 of the machine knob on its 0–10 scale [10]. To obtain representative pore size distribution curve for the concrete in a particular beam, the results of six porosimetry data were averaged. For this purpose, the intruded volumes of mercury for all the six samples at a particular radius of the pore were averaged to obtain average intruded volume of mercury at that pore radius. This procedure was repeated at a large number of radii to generate the resulting average pore size distribution curve.

2.7. Results

In situ strength of concrete in all 36 beams was estimated according to the procedure stated. From the intrusion curves of six samples collected from a beam, average intrusion curve was obtained for concrete in each beam. Thus, 36 such average intrusion curves were produced [11]. The apparent porosity of the concrete (corresponding to 33,000 psi intrusion pressure) for each of the six samples taken from a beam was calculated using the individual cumulative intrusion volume and the relevant weight measurements for a sample, and averaged. Average apparent porosity of concrete in each of the 36 beams was thus obtained. From the average intrusion curves, the values of mean distribution radius, r_m, was estimated according to the equation given below [23]:

$$\ln r_m = \frac{\sum_{i=1}^{i=n} V_i \ln r_i}{\sum_{i=1}^{i=n} V_i} \tag{3}$$

where, for the continuous intrusion curve divided into n discrete radii ranges, V_i is the incremental intrusion of mercury corresponding to ith radius range represented by the mean radius r_i. The porosity belonging to the pore size ranges greater than 106, 53–106 and 10.6–53 nm, and less than 10.6 nm is also calculated from these intrusion curves. These results along with in situ strength of concrete in beams are presented in Table 2.

3. Appraisal of existing models

Quite a few relationships involving strength and porosity of cement-based materials have been reported in literature. Notable among them are linear relationship of the form $\sigma = \sigma_0 - Kp$, power exponent relationship of form $\sigma = \sigma_0(1-p)^m$, exponential relationship of the form $\sigma = \sigma_0 e^{-Kp}$ and $\sigma = K\ln(p_{0s}/p)$. In all these relationships, σ stands for compressive strength at porosity p, σ_0 stands for compressive strength at zero porosity, p_{0s} stands for porosity at zero strength, m and K are empirical constants. On plotting the compressive strength of concrete given in Table 2 against their respective apparent porosity, it was observed that there are two distinct clusters of points. One cluster corresponds to concrete made with quartzite aggregates and the other corresponds to brick aggregates. The best-fit linear curve of the form $\sigma = \sigma_0 - Kp$ between the strength and apparent porosity, for both the clusters of points taken together, yields $\sigma = 34.25 - 0.615p$, with a coefficient of correlation C_r =53%. Similarly, when the strength porosity data for the concrete made with quartzite aggregates were used alone, the resulting equation becomes $\sigma = 53.45 - 2.301p$, with a coefficient of correlation C_r = 52%. Poor correlation is exhibited in both cases; thus, linear relationship of the form $\sigma = \sigma_0 - Kp$, suggested by Hasselman [24], seems to be oversimplified. Two values of σ_0 estimated as above differ quite significantly from each other and apparently depend on aggregate type. Results of regression for other forms of relationship are given in Table 3 and

Table 2
In situ strength, porosity, mean distribution radius, etc., of concrete

Beam number	Mix	Age, curing (day)	Exposure condition	In situ strength (MPa)	Apparent porosity (%)	r_m (nm)	Porosity in pore size range (%)			
							>106 nm	53–106 nm	10.6–53 nm	<10.6 nm
1	Mix1	28, 27	Atm.	18.3	12.96	34.3	3.931	1.084	4.907	3.038
2	Mix2	28, 27	Atm.	28.4	11.93	38.7	4.388	0.946	3.728	2.868
3	Mix2	28, 1	Atm.	26.8	10.87	58.7	5.166	0.898	2.639	2.163
4	Mix2	28, 27	300 °C	22.7	11.10	41.3	4.388	0.816	3.840	2.065
5	Mix2	28, 27	600 °C	21.5	13.53	42.3	5.006	1.001	4.376	3.147
6	Mix2	28, 27	Acidic	27.5	12.75	26.6	3.036	1.258	5.060	3.391
7	Mix2	84, 27	Atm.	29.7	10.80	39.3	3.965	0.816	3.515	2.504
8	Mix2	84, 1	Atm.	26.8	10.83	52.9	4.867	0.895	2.741	2.322
9	Mix3	28, 27	Atm.	30.3	11.80	45.8	4.085	1.344	4.569	1.802
10	Mix4	28, 27	Atm.	35.3	11.22	31.2	3.252	0.813	4.444	2.711
11	Mix5	28, 27	Atm.	40.3	11.50	30.4	3.175	0.907	4.536	2.882
12	Mix6	28, 27	Atm.	43.2	9.26	28.1	2.592	0.830	3.573	2.265
13	Mix6	28, 27	300 °C	38.7	10.38	41.9	4.018	0.746	3.586	2.030
14	Mix6	28, 27	600 °C	28.3	16.55	34.2	5.125	1.121	5.979	4.325
15	Mix6	28, 27	Acidic	42.5	9.50	23.0	1.894	0.839	4.032	2.735
16	Mix6	84, 1	Atm.	39.3	9.63	30.3	2.497	0.849	3.643	2.639
17	Mix7	28, 27	Atm.	14.2	33.70	146.9	22.06	3.014	4.764	3.860
18	Mix8	28, 27	Atm.	16.4	33.14	126.7	20.18	3.490	5.400	4.067
19	Mix1	28, 27	Atm.	15.5	11.22	41.6	4.163	0.717	3.830	2.510
20	Mix2	28, 27	Atm.	24.0	12.04	35.4	3.656	0.996	4.539	2.849
21	Mix2	28, 1	Atm.	23.2	11.39	71.3	5.719	0.870	3.083	1.718
22	Mix2	28, 27	300 °C	14.9	12.23	31.2	3.938	0.902	3.743	3.642
23	Mix2	28, 27	600 °C	13.6	15.37	49.6	6.287	1.369	4.443	3.271
24	Mix2	28, 27	Acidic	23.7	12.01	30.5	3.408	1.118	4.474	3.010
25	Mix2	84, 27	Atm.	25.7	10.38	47.5	4.140	0.739	3.371	2.130
26	Mix2	84, 1	Atm.	23.9	10.40	68.3	4.999	0.802	3.021	1.578
27	Mix3	28, 27	Atm.	30.7	11.30	43.0	3.849	0.997	4.404	2.050
28	Mix4	28, 27	Atm.	33.8	13.55	45.0	5.159	0.936	4.999	2.460
29	Mix5	28, 27	Atm.	37.7	11.85	29.3	3.091	0.840	5.152	2.767
30	Mix6	28, 27	Atm.	35.4	9.90	36.9	3.432	0.709	3.546	2.213
31	Mix6	28, 27	300 °C	28.8	9.92	43.6	3.672	0.630	3.699	1.919
32	Mix6	28, 27	600 °C	24.2	13.31	36.9	4.108	0.986	5.229	2.983
33	Mix6	28, 27	Acidic	36.2	9.28	35.0	2.622	0.761	4.088	1.805
34	Mix6	84, 1	Atm.	36.3	9.54	35.9	3.097	0.552	3.618	2.270
35	Mix7	28, 27	Atm.	17.7	33.60	122.1	20.05	3.897	5.327	4.330
36	Mix8	28, 27	Atm.	19.6	31.70	109.7	18.08	3.291	5.740	4.579

were obtained using the data of the concrete made with quartzite aggregate only.

Poor correlation is observed for all the above forms of curve and it appears that simple strength–porosity relationships are not applicable in this case. In Fig. 2, these curves are shown together with the data used for curve fitting. Regression for the above forms of curve using data for both aggregates taken together results in even poorer correlation. Thus, simple relationships involving only porosity are inadequate in explaining the observed variation of in situ strength of concrete with measured apparent porosity.

A completely different form of strength–porosity relationship was originally proposed by Older and Rößler [25] and was further modified by Atzeni et al. [23]. A slightly modified form of this relationship is:

$$\sigma = \sigma_0 - ap_{>106\ \mathrm{nm}} - bp_{106-53\ \mathrm{nm}} - cp_{53-10.6\ \mathrm{nm}} - dp_{<10.6\ \mathrm{nm}} \quad (4)$$

where σ and σ_0 have the same meaning as defined earlier, and a, b, c and d are the constant coefficients in the equation. $p_{>106\ \mathrm{nm}}$ is the porosity with radius r>106 nm, $p_{106-53\ \mathrm{nm}}$ is the porosity between pore radius 53 and 106 nm, $p_{53-10.6\ \mathrm{nm}}$ is the porosity between pore radius 10.6 and 53 nm and $p_{<10.6\ \mathrm{nm}}$ is the porosity with radius r<10.6 nm.

Considering all the data presented in Table 2, inclusive of both types of aggregates, the multiple linear regression yielded the values of the various coefficients as: σ_0 = 32.09, a = 1.135, b = − 4.343, c = − 1.993 and d = 4.942. Similar to the observations made earlier for cement pastes by Atzeni et al. [23], two coefficients b and c are negative, in-

Table 3
Results of regression for simple relationships

Form of equation	Equation	C_r (%)
$\sigma = K\ln(p_{0s}/p)$	$\sigma = 37.1\ln(0.284/p)$	55
$\sigma = \sigma_0(1-p)^m$	$\sigma = 68.74(1-p)^{8.15}$	54
$\sigma = \sigma_0 e^{-Kp}$	$\sigma = 74.4e^{-8.96p}$	51

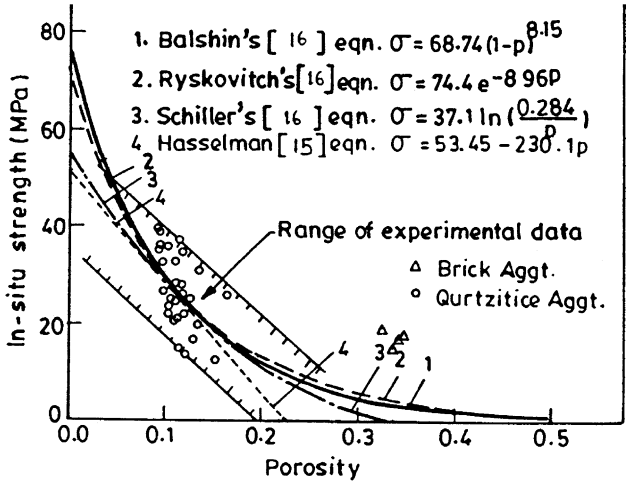

Fig. 2. Strength–porosity relationships.

dicating that increased pore volume in certain size ranges of pores increases the strength of concrete. Difficulty in explaining the negativity of coefficients led to rejection of this model by Atzeni et al. [23] in the past. Thus, this type of relationship is also unsuitable for correlating in situ strength of concrete with its measured pore size characteristics.

3.1. Relationship of Atzeni et al. [23]

The relationship of Atzeni et al. relating strength of cement pastes with its porosity, strength at zero porosity, etc., is given as:

$$\sigma = K\frac{\sigma_0(1-p)}{\sqrt{r_m}}. \tag{5}$$

In this equation, σ, σ_0, p and K have the same meaning as defined earlier. To consider the effect of pore size distribution on strength, the authors used a parameter r_m in the relationship and termed it as mean distribution radius, as defined earlier in Eq. (3). Atzeni et al. [23] advocated the estimation of σ_0 from linear strength–porosity relationship; however, the analysis presented in Section 2 demonstrates that this estimation is likely to be grossly erroneous; thus, to start with, the in situ strength is plotted against $(1-p)/\sqrt{r_m}$, as shown in Fig. 3. Using the data for quartzite aggregate alone, the best-fit linear curve between in situ strength and $(1-p)/\sqrt{r_m}$, is $\sigma = 189.3(1-p)/\sqrt{r_m} + 2.45$. In this equation, p is in fraction, r_m is in nanometer and σ is in megapascal. However, the intercept 2.45 is relatively small and from physical consideration, when $p \to 1$ or $(1-p) \to 0$, r_m tends to be large ($r_m \to \infty$), resulting in $[(1-p)/\sqrt{r_m} \to 0]$; therefore, for $p \to 1$, σ must be negligibly small $[\sigma \to 0]$. Thus, the curve between σ and $(1-p)/\sqrt{r_m}$ can be fitted through the origin. The coefficient of correlation of this linear plot is 70%. The coefficient of correlation, estimated for nonlinear relationships between above two variables, was lower than above.

3.2. Strength–porosity relationship of Luping [26]

In this model, pores are divided into different size groups and the fracture process is simulated through a computer model. The basic theory underlying the model is available in the literature [26]. For a given portion of material containing the ith pore size group, the limiting condition of failure is given by the following inequality:

$$\sigma_{cri} \geq \sqrt{\frac{K_m A_{mi}}{r_i}} \tag{6}$$

where A_{mi} represents the fraction of solid (material) and can be represented as $A_{mi} = 1 - 4r_i N_i(1 - r_i N_i)$, N_i represents the number of pores of ith size group per unit side length of the overall material, r_i is the mean pore radius of the group and K_m is an empirical constant that includes the modulus of elasticity of material at zero porosity and the surface energy, etc. The model assumes a specific regular geometrical arrangement of pores in all three spatial directions. The material is assumed to fracture progressively with applied stress, starting from the fraction containing the largest pores to that containing the smallest pores. The stress it withstands at the final stage of fracture is assumed as the strength of the material.

To evaluate the strength of concrete from its pore size distribution data obtained through MIP, the knowledge of the constant K_m for concrete in Eq. (6) is essential. In the absence of information on K_m evaluation of this model for its applicability to the relationship among strength, porosity and pore size distribution for concrete is rather difficult. However, values of K_m can be evaluated if strength and porosimetry data are available. Starting from the finest pore size group and the strength of the material, values of K_m can

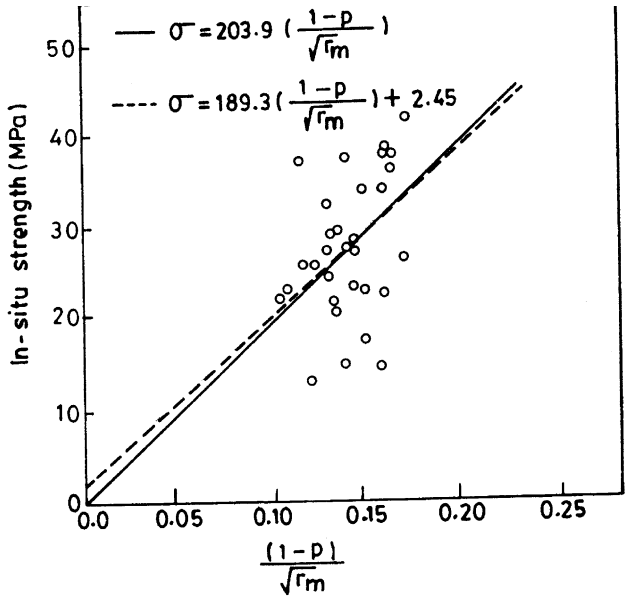

Fig. 3. Relationship between in situ strength and $\left(\frac{1-p}{\sqrt{r_m}}\right)$.

be estimated from Eq. (6) through an inverse computation process suggested by the authors.

K_m includes the effect of modulus of elasticity and surface energy of concrete at zero porosity, and thus strongly depends on the nature of pore free solid. The nature of solid again is dependent on cement content of the concrete. Thus, a plot of K_m values against cement content expressed as fraction is shown in Fig. 4 for concrete exposed to ambient laboratory temperature and cured for 27 days in standard manner. The resultant fitted linear equation is $K_m = 54{,}402.1C - 4255.5$, with a coefficient of correlation equal to 90%. It can be observed that at the cement content (expressed as fraction of total weight) of 0.078, the value of K_m is zero and, consequently, the strength of concrete is also zero. Thus, this is the minimum possible cement content for concrete. Within the range of cement content and w/c ratio used in this work, the solid matrix strength of concrete is independent of porosity and, hence, is also independent of w/c ratio. The matrix strength increases with increase in cement content. Thus, K_m can be estimated through the equation obtained for the concrete prepared with the given aggregate and cement used. An elaborate discussion on the subject, however, is available elsewhere [11].

3.3. Discussions on the applicability of existing models

Analysis presented in the previous subsections demonstrate that both simple strength–porosity relationship and Older and Rößler [25] types of models are inadequate in explaining the variation of in situ strength of concrete with apparent porosity and pore size distributions. The model of Atzeni et al. [23], on the other hand, is able to explain the above behaviour better. Luping's model is the most complicated among all the models discussed. In the absence of the value of the empirical constant K_m, it is difficult to make even relative assessment of strength through this model.

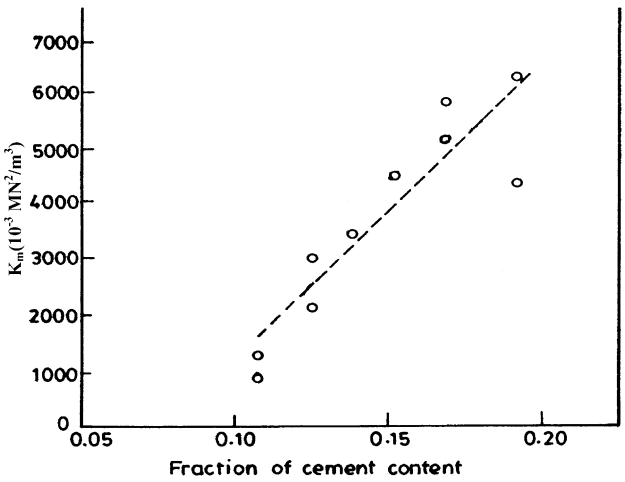

Fig. 4. K_m versus fraction of cement contents of concretes.

4. Proposed model

4.1. Basic model

Compared to other models, the model of Atzeni et al. [23] exhibited a somewhat better degree of correlation between the strength and independent variable defined. This can be partially explained through Griffith's theory. According to Griffith's theory, the critical stress resulting in rapid growth of crack and fracture causing failure under tension is given by:

$$\sigma_t = \sqrt{\frac{2ET}{\pi c_1}} \tag{7}$$

where E, T and c_1 stand for modulus of elasticity, fracture surface energy of the material and half-crack length, respectively. For a porous material like concrete containing pores of different sizes, E and T are effective modulus of elasticity and effective fracture surface energy, respectively, for the uncracked overall material consisting of solid matrix and the pore [16,26,27]. For porous materials, the effective modulus of elasticity is a function of porosity, as pores do not contribute to elastic modulus. Numerous models relating the porosity and elastic modulus are available [4,15–17,26]. The simplest one is the linear form, $E = E_0(1-p)$. The fracture surface energy is the energy required for creating a unit area of interface between the solid and air [4,16,17,27]. For porous material, the interface between the solid and air already exists at pores; however, for pore free solid portion, the same needs to be created. The effective fracture surface energy required for fracture of gross unit area of porous material, thus, will be lower with increase in porosity. This has been recognized in the past by Brandt [16] and Wittmann [27] and relationships between effective fracture surface energy and porosity have been proposed for concrete and other cement-based materials. The simplest form of this relationship is again linear, namely, $T = T_0(1-p)$. The effective modulus of elasticity (E) and the effective fracture surface energy (T) of concrete are thus dependent on the porosity, since only solid contributes to them. Assuming simple linear models and assuming the effective half-crack length as the average radius of the pores estimated through the mean distribution radius [23,26], the resulting equation for the tensile strength at the onset of fracture can be expressed as:

$$\sigma_t = \sqrt{\frac{2E_0T_0}{\pi}}\frac{(1-p)}{\sqrt{r_m}} \tag{8}$$

where E_0 and T_0 represent the modulus of elasticity and specific surface energy of pore free solid, respectively. This model is similar to that suggested by Wittmann [27] except that the effective modulus of elasticity is also assumed to be proportional to $(1-p)$. It may be mentioned here that other complex forms of relationship involving E, T and p reported

in literature, when tried, were unable to explain the empirically observed behavior (Fig. 3) better than the model of Atzeni et al.

The uniaxial compressive strength of the material is dependent on the tensile fracture strength of the material; therefore, the same can be written as:

$$\sigma = K_1 \frac{(1-p)}{\sqrt{r_m}}. \quad (9)$$

Empirical constant K_1 takes care of E_0, T_0 and other unaccounted factors. E_0, modulus of elasticity of solid pore free matrix, depends on the binder content of the concrete. T_0, the energy required to create unit surface area of solid matrix of concrete, is dependent on the bond strength of the concrete–particulate system. Estimated modulus of elasticity of unhydrated cement particles is comparable to that of natural rock. Hydration of cement, on the other hand, results in an increase in Van der Waals forces, causing an increase in the modulus of elasticity of solid matrix [17]. As a first approximation, therefore, both E_0 and T_0 can be assumed to be directly proportional to the cement content of concrete for the range of mix proportions considered; hence, Eq. (9) can be rewritten as:

$$\sigma = K_2 C \frac{(1-p)}{\sqrt{r_m}} \quad (10)$$

where C is the cement content of mix, expressed as fraction. The fitted linear equation between in situ strength and $C(1-p)/\sqrt{r_m}$ passing through the origin for all the data, as shown in Fig. 5, results in a value of 1294.3 for K_2. The coefficient of correlation for this equation is estimated to be 90%, which shows a considerable improvement over original relationship of Atzeni et al. discussed earlier.

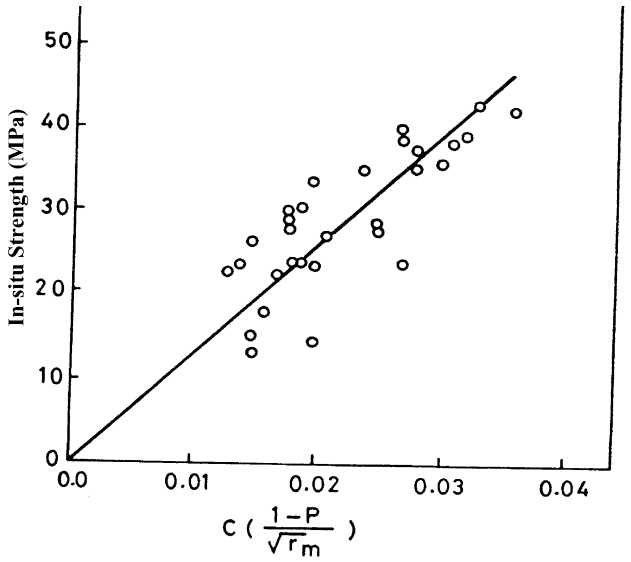

Fig. 5. In situ strength versus $C\left(\frac{1-p}{\sqrt{r_m}}\right)$.

4.2. Effects of age, exposure condition and aggregate type

Exposure to temperature or acidic environment results in irreversible changes in cement hydrates, resulting in alteration of effective binder content of the concrete. Taking into account the effective binder content present after exposure to various environments, different multiplying factors f_e, f_a and f_T can be introduced in the above equation. The factors f_e, f_a and f_T take into consideration the effects of exposure to acidic environment, age and temperature, respectively. When soft porous aggregates are used in the concrete instead of hard rocks (quartzite), as in this work, the mode of failure of concrete under compressive load differs considerably. For concrete prepared with strong hard aggregates, the observed fracture surface passed through the mortar–aggregate interface and crushing of aggregate was absent. While for concrete prepared with Mix7 and Mix8, the crushing of aggregate was always observed during compression tests. Besides, higher porosity of concrete was observed for soft aggregate prepared with identical mix proportions due to the contribution from porous aggregate itself. Therefore, type of aggregate also influences the void free matrix property, and hence, a multiplying factor f_{ca} can be also introduced for aggregate type in Eq. (10). Thus, on further modification, Eq. (10) can be rewritten as:

$$\sigma = \kappa f_{ca} f_e f_a f_T C \frac{(1-p)}{\sqrt{r_m}}. \quad (11)$$

In the above equation, κ is the new empirical constant. To evaluate f_T, the following procedure was adopted. The concrete samples prepared from only Mix2 and Mix6 were subjected to elevated temperatures (300 and 600 °C). Thus, the value of K_2 defined in Eq. (10) for all the 27-day-cured and 28-day-old Mix2 and Mix6 concrete samples exposed to room temperature, 300 and 600 °C were estimated and averaged for two modes of compaction. The average value so obtained was then divided by the K_2 value corresponding to 26 °C to obtain a ratio corresponding to each temperature. This ratio for both mixes at 26 °C, therefore, is unity. The average of the ratio for two mixes is the f_T value corresponding to a given temperature. The best-fit linear curve between f_T and temperature results in a simple equation: $f_T = 1 - 3.5 \times 10^{-4}(T-26)$, where T is the exposure temperature (°C) of concrete. The values of f_e and f_a were also deduced in the same manner for 84 days of exposure to acidic and atmospheric environments, respectively. The values obtained are 0.91 and 1.1 for f_e and f_a, respectively. The values of factors f_e, f_T and f_a are unity for moist-cured 28-day-old concrete exposed to 26°C temperature only. Values of f_e for other environments can be evaluated by adopting a similar methodology when data are available. As per standard practice, IS: 456 [28], etc., the age factor for 3-month-old concrete nearly coincides with the f_a value estimated and thus validates the estimation of the same. Similar factor for inadequate curing can also be introduced

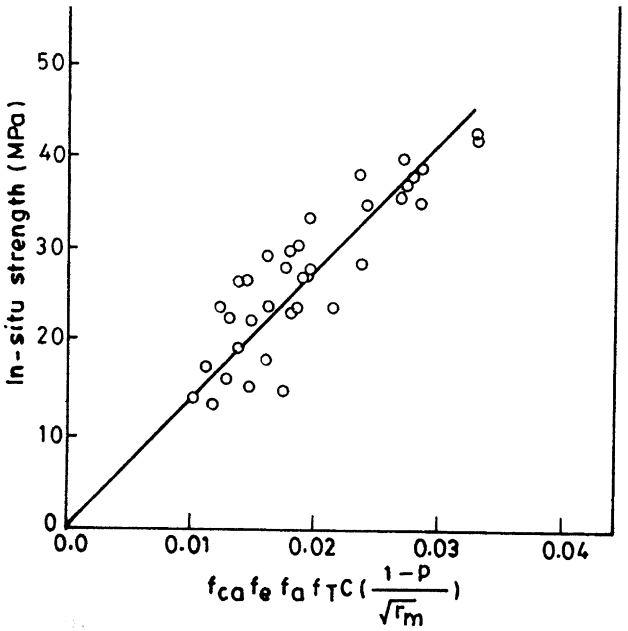

Fig. 6. In situ strength versus $f_{ca}f_ef_af_TC\left(\frac{1-p}{\sqrt{r_m}}\right)$.

in Eq. (10); however, due to lack of sufficient data, this exercise was not undertaken in the present work. It may be noted here that expressions for f_T and f_e are obtained through relatively small set of data; thus, more reliable expressions for f_T and f_e can be arrived at using the same methodology when a larger data set becomes available.

To evaluate the value of factor f_{ca} for soft, crushed brick aggregates, the ratios of actual in situ strength to strength of concrete estimated through Eq. (10), in beams prepared with Mix7 and Mix8, are calculated. These ratios are 1.72 and 1.96 for mechanically and manually compacted concrete, respectively, for Mix7. Similarly, the ratios for Mix8 concrete are 1.58 and 1.71, respectively. The average of the above four values (1.74) represents f_{ca} for crushed brick aggregate. The value of f_{ca} for quartzite aggregate is unity.

A final plot of in situ strength against the factor, $\{f_{ca}f_ef_af_TC(1-p)/\sqrt{r_m}\}$, is given in Fig. 6. The resulting best-fit line yields a value of 1.39×10^3 for κ and the coefficient of correlation is 85%. It is interesting to note that the coefficient of correlation for the above best-fit line, considering the data for concrete made with quartzite aggregate alone, i.e., with $f_{ca}=1$, is 92%.

5. Conclusions

1. A large set of data on apparent porosity, pore size distribution and in situ strength of concrete has been presented for concrete of varying mix proportions.
2. It has been demonstrated through an appraisal that most of the existing models relating the strength with pore size characteristics of cement-based material are inadequate in the context of concrete.
3. A new model has been proposed, which takes into account the apparent porosity, pore size characteristics and cement content of concrete, etc., in addition to aggregate type, exposure condition and age of concrete.

Acknowledgements

The authors acknowledge CSIR, HRD Group of the Government of India, for providing the financial support for carrying out the research.

References

[1] T.S. Nagraj, B. Zahida, Generalization of Abrams' laws, Cem. Concr. Res. 26 (6) (1996) 933–942.
[2] G.M. Därr, U. Ludwing, Determination of permeable porosity, Mater. Struct. 6 (2) (1973) 185–190.
[3] F.S. Rostasy, R. Weib, G. Wiedemann, Changes of pore structure of cement mortar due to temperature, Cem. Concr. Res. 10 (2) (1980) 157–164.
[4] I. Soroka, Portland Cement Paste and Concrete, Macmillan, London, UK, 1979.
[5] D. Winslow, D. Liu, Pore structure of paste in concrete, Cem. Concr. Res. 20 (2) (1990) 227–235.
[6] H.W. Reinhardt, in: A. Aguado, R. Gettu, S.P. Shah (Eds.), Concrete Technology: New Trends Industrial Applications, E & FN Spon, UK, 1995, pp. 19–32.
[7] P.K. Mehta, Concrete: Structure, Properties and Materials, Prentice-Hall, New York, 1986.
[8] S. Popovics, New formulas for the prediction of the effects of porosity on concrete strength, ACI Mater. J. 78 (2) (1981) 127–129.
[9] S. Popovics, Generalization of Abrams' law, ACI Mater. J. 82 (2) (1985) 136–146.
[10] A.I. Laskar, R. Kumar, B. Bhattacharjee, Some aspects of evaluation of concrete through mercury intrusion porosimetry, Cem. Concr. Res. 27 (1) (1997) 93–105.
[11] R. Kumar, Strength and permeation quality of concrete through mercury intrusion porosimetry, PhD Thesis, Department of Civil Engineering, Indian Institute of Technology Delhi, New Delhi, India, 1997.
[12] R. Kumar, B. Bhattacharjee, Study on some factors affecting the results in the use of MIP method in concrete research, Cem. Concr. Res., USA (submitted for publication).
[13] D.N. Winslow, S. Diamond, A mercury porosimetry study of the evaluation of porosity in Portland cement, ACI J. Mater. 5 (3) (1970) 564–585.
[14] S. Diamond, A critical comparison of mercury intrusion porosimetry and capillary condensation pore size distribution of Portland cement pastes, Cem. Concr. Res. 1 (5) (1971) 531–545.
[15] A.M. Neville, J.J. Brooks, Concrete Technology, Longman, Singapore, 1990.
[16] A.M. Brandt, Cement Based Composites: Materials, Mechanical Properties and Performance, E & FN Spon, UK, 1995.
[17] K. Newman, Concrete systems, in: L. Holliday (Ed.), Composite Materials, Elsevier, USA, 1966, pp. 336–452.
[18] S. Diamond, Mercury porosimetry; an inappropriate method for the measurement of pore size distributions in cement-based materials, Cem. Concr. Res. 30 (10) (2000) 1517–1525.
[19] IS: 516, Methods of Tests for Strength of Concrete, BIS (Bureau of Indian Standards), India, 1956.
[20] BS 1881: Part 120, Method for Determination of the Compressive Strength of Concrete Cores, British Standard Institution (BSI), UK, 1983.

[21] E.J. Sellevold, Mercury porosimetry of hardened cement paste cured or stored at 97 °C, Cem. Concr. Res. 4 (3) (1974) 399–404.
[22] D.H. Bager, E.J. Sellevold, Mercury porosimetry of hardened cement pastes: the influence of particle size, Cem. Concr. Res. 5 (2) (1975) 171–175.
[23] C. Atzeni, L. Massidda, U. Sanna, Effect of pore size distribution on strength of hardened cement pastes, Proceedings of the First International RILEM Congress on Pore Structure and Material Properties, Paris, 1987, pp. 195–202.
[24] D.P.H. Hasselman, Relation between effects of porosity on strength and Young's modulus of elasticity of polycrystalline materials, J. Am. Ceram. Soc. 46 (11) (1963) 564–565.
[25] I. Older, M. Rößler, Investigations on the relationship between porosity, structure and strength of hydrated Portland cement pastes: ii. Effects of pore structure and degree of hydration, Cem. Concr. Res. 15 (4) (1985) 401–410.
[26] T. Luping, A study of the quantitative relationship between strength and pore size distribution of the porous materials, Cem. Concr. Res. 16 (1) (1986) 87–96.
[27] F.H. Wittmann, Fracture Mechanics of Concrete, Elsevier, Amsterdam, 1983, pp. 56–62.
[28] IS: 456, Indian Standard Code of Practice for Plain and Reinforced Concrete, 3rd ed., BIS (Bureau of Indian Standards), India, 1978.